Poster P-150 has been designated as a Distinguished Poster at Display Week 2025. The full-length version of this paper appears in a Special Section of the *Journal of the Society for Information Display (JSID)* devoted to Display Week 2025 Distinguished Papers. This Special Section will be freely accessible until December 31, 2025 via:

https://sid.onlinelibrary.wiley.com/doi/full/10.1002/jsid.2082

Authors that wish to refer to this work are advised to cite the full-length version by referring to its DOI:

https://doi.org/10.1002/jsid.2082

Mechanically Stable, Stretchable Ferroelectric Thin-Film Transistors for Display Application

Heonbang Lee, Junmi Lee*, Jaein Noh* and Jin Jang**

Advanced Display Research Center, Department of Information Display, Kyung Hee University, Seoul 02447, South Korea

Abstract

We present ferroelectric thin-film transistors (FE-TFTs) with a metal-insulator-semiconductor-ferroelectric (MISF) structure on polyimide (PI) and polydimethylsiloxane (PDMS) substrate. The memory window is 9.1 V and can operate under a 1 mm bending radius. Its biaxial stretchability is 30%. We proposed a 3T0C pixel circuit without a capacitor for the PWM mode of micro-LED displays using FE-TFTs.

Author Keywords

spray pyrolysis; ferroelectric thin-film transistor (FE-TFT); zirconium oxide (ZrO_2); flexible & stretchable electronics

1. Introduction

Flexible electronic devices such as flexible displays, electronic skins, and implantable devices, are gaining increasing attention for their portability, lightweight design, and adaptability to human use. (1-4) Ferroelectric field-effect transistors (FeFETs) are particularly promising for these applications due to their low power consumption, and high-speed operation. (5-7) However, mechanical strain may lead to a dielectric breakdown due to internal defect formation, posing a challenge to device reliability. (8)

Among the ferroelectric materials, fluorite-based films have gained significant attention because of their advantages such as environmental friendliness, large band gap, and simplified structure. (9) Zirconium oxide (ZrO_2) has been widely investigated due to its low crystallization temperature. (10,11) Note that the ferroelectric properties of ZrO_2 can be shown in wide thickness ranges with large process margins. (12) For flexible substrates, polyimide (PI) substrates are widely used for flexible displays because of their excellent mechanical and thermal stability and manufacturing capabilities. (1,3) Recent research has demonstrated the direct growth of HZO films on PI substrates for low-voltage nonvolatile transistors. (6) Additionally, PI can be combined with polydimethylsiloxane (PDMS) substrates to enhance mechanical properties, enabling the development of stretchable thin-film transistors (TFTs). (13)

The process compatibility with the conventional switching transistors is important for applying the FE devices. Previous research has demonstrated the fabrication of ferroelectric capacitors or transistors on CMOS backplanes. However, the complexity of this approach leads to an ongoing need for simplified and efficient fabrication methodologies. (14)

This work proposes a mechanically stable, metal-insulator-semiconductor-ferroelectric (MISF) structured ferroelectric thin-film transistor (FE-TFT) deposited by spray pyrolysis on PI and PDMS substrates. The spray-pyrolyzed ZrO_2 shows crystalline o-phase formation. The ferroelectric behavior of the device is achieved by ferroelectric coupling of the ZrO_2 layer. The TFT shows a large memory window (MW) of 9.1 V at ± 15 V gate voltage (VGS) sweep, with good temperature stability. The device could be operated well under 1 mm bending radius (R).

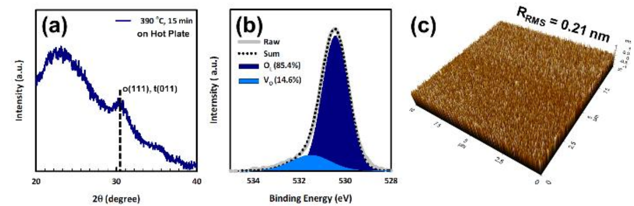

Figure 1. ZrO_2 thin film characterization. (a) The GIXRD spectra, (b) XPS O1s spectra, and (c) surface morphology by AFM measurements.

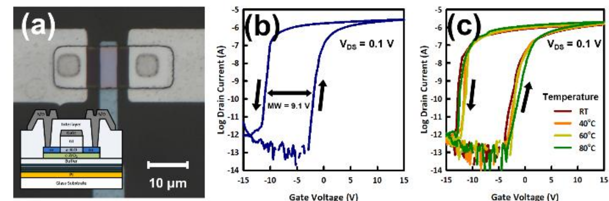

Figure 2. Electrical characterization of the FE-TFTs. (a) Optical image of the fabricated device with W/L of 10 μm/6 μm. The inset depicts the cross-sectional view of the FE-TFT. (b) The hysteresis curve at a ± 15 V V_{GS} sweep. (c) Hysteresis curve with various temperatures.

The TFTs were transferred onto PDMS substrates for stretchability. The stretchable TFT shows a stable operation for 100 h in a 30 % biaxially stretched condition. The 3T0C pixel circuit was made based on the MISF TFT. The switching oxide-TFTs (SW-TFTs) were made without the ferroelectric layer, with the MISF process. The 3T0C pixel circuit was used for the PWM mode of micro-LED displays. The proposed ferroelectric MISF TFTs could be used for next-generation, flexible, and stretchable display devices.

2. Experimental Section

A precursor solution of 0.15 M ZrO_2 was prepared by dissolving Zirconium (IV) acetylacetonate ($Zr(C_5H_7O_2)_4$, 97%) in a mixed solvent of Dimethylformamide (C_3H_7NO, ≥ 99.75%) and Methanol (CH_3OH, ≥ 99.9%) with 7:3 ratio. The precursor solution was prepared in an N_2 environment and stirred at 70 °C for 8 hrs. A 0.45 μm PTFE syringe filter was used to eliminate residual particles from the precursor solution before spray coating.

The fabrication process of flexible MISF FE-TFTs on polyimide substrate is as follows. First, the carbon nanotube/graphene oxide sacrificial layer was deposited by spray pyrolysis. Then, PI was coated to 10 μm and cured at 450 °C for 2 h. After the deposition of the gas barrier and buffer oxide layer consisting of SiO_2/SiN_x multilayer by plasma-enhanced chemical vapor deposition (PECVD) at 420 °C, a 30 nm thick ZrO_2 layer was deposited by spray pyrolysis at the temperature of 370 °C using a Lab Spray Coater (ReVo-S). During spray coating, the distance between the substrate and the spray nozzle was maintained at 10.0 cm, and the

ISSN 0097-996X/25/5603-2018-$1.00 © 2025

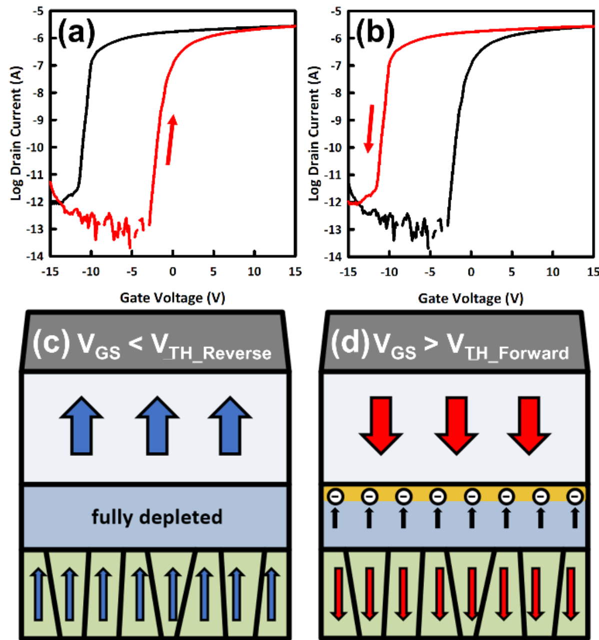

Figure 3. Operational mechanism of the proposed FE-TFTs. (a), (b) The hysteresis curves and (c), (d) carrier concentrations in the active layer and electrical force induced by the dipole orientation in FE layer.

nozzle's moving speed was set at 7.0 cm s^{-1}. The flow rate of precursor solution during spray remained constant at approximately 2.5 mL min^{-1}. The film was treated with 2 cycles of Ar/O_2 plasma and annealed on a hot plate at 390 °C for 15 mins in air. Then, 10 nm amorphous indium gallium oxide (a-IGO) was deposited at room temperature by sputtering as an active layer. A 100 nm thick SiO_2 and 100 nm thick Mo were deposited as a gate insulator (GI) and gate electrode by PECVD and sputtering, respectively. The doping region was formed by a self-aligned process utilizing a gate electrode as a photomask. A 300 nm thick SiO_2, and 150 nm thick Mo were deposited as interlayer and source/drain (S/D) electrodes, respectively. Finally, the TFTs were annealed in a vacuum furnace at 250 °C for 2 hrs.

The electrical characteristics of the FE-TFTs were analyzed by an Agilent 4156C semiconductor parameter analyzer. The threshold voltage (V_{TH}) was defined as the gate voltage (V_{GS}) corresponding to constant drain current (I_{DS}) of W/L x 10 pA at drain voltage (V_{DS}) of 0.1 V, where W is channel width and L is length. The memory window was calculated by the difference of V_{TH} of the forward sweep ($V_{TH_Forward}$) and the reverse sweep ($V_{TH_reverse}$) from the voltage sweeping hysteresis measurements. The μ_{FE} was calculated by transconductance; $\mu_{FE} = L/(WC_{OX}V_{DS})\, g_{m_max}$, where C_{OX} is the capacitance of the gate dielectric and g_{m_max} is the maximum transconductance.

3. Results and Discussion

The properties of ZrO_2 films by Ar/O_2 plasma treatment and sequent crystallization were analyzed. **Fig. 1(a)** shows the grazing incidence X-ray diffraction (GIXRD) spectra of the ZrO_2 film. The peak was shown at 30.4 ° indicating an orthorhombic phase formation in ZrO_2. (11) **Fig. 1(b)** shows the O1s spectra of X-ray photoelectron spectroscopy (XPS) resulting from the surface of the ZrO_2. The metal-oxygen bonds and the oxygen vacancies were calculated as 85.4% and 14.6 % respectively. The oxygen-related defects were effectively suppressed by Ar/O_2 plasma

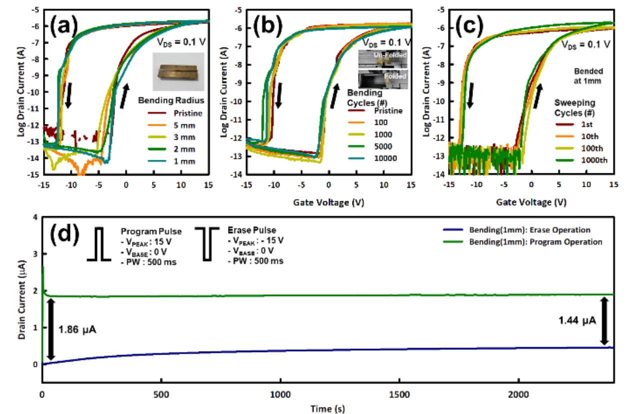

Figure 4. Mechanical stabilities of the FE-TFT. Hysteresis curves with (a) bending radius down to 1 mm, (b) bending tests up to 10000 cycles at R = 3 mm, and (c) endurance measurements of up to 1000 times of ± 15 V V_{GS} sweep at R = 1 mm. (d) Retention characteristics measured up to 2400 s at R = 1 mm. The insets show the pulse conditions for the program and erase pulses.

Table 1. The comparison of the structural and mechanical properties of flexible FE-TFTs.

Structure	Deposition Method	Ferroelectric Material	Flexible Substrate	Minimal Bending Radius	Year (Ref.)
MFS	ALD	$Hf_{0.5}Zr_{0.5}O_2$	MICA	4 mm	2020 (5)
MFIS	Spin Coating	$Hf_{0.5}Zr_{0.5}O_2$	PI	2 mm	2022 (6)
MFS	ALD	$Hf_{0.5}Zr_{0.5}O_2$	MICA	5 mm	2024 (7)
MISF	Spray Pyrolysis	ZrO_2	PI	1 mm	This Work

treatment. (15) The root-mean-square surface roughness (R_{RMS}) of 0.21 nm by the atomic force microscopy (AFM) measurements are shown in **Fig. 1(c)**.

Fig. 2(a) shows an optical image of MISF TFT. The electrical characteristics were measured with the TFT of W = 10 μm and L = 6 μm. The inset shows the cross-sectional view of the MISF TFT. **Fig. 2(b)** shows a counter-clockwise hysteresis curve measured with MW = 9.1 V at a ± 15 V V_{GS} sweep. The drain voltage (V_{DS}) of 0.1 V was used for the measurement to minimize the drain bias effect which can affect the dipole orientation. **Fig. 2(c)** shows hysteresis curves with rising temperatures of up to 80 °C. The $V_{TH_Forward}$ tends to shift slightly in a positive direction indicating some charge trapping. (15)

The operational mechanism is depicted in **Fig. 3**. **Fig 3(a) and (b)** highlight the forward and reverse sweep respectively. **Fig. 3(c)** and (d) show the ferroelectric dipole orientation and carriers in the active layer. By ferroelectric coupling, the dipoles can induce repulsive/attractive force to the charge carriers, and affect the carrier concentration at the channel region. (16,17) The forward sweep operation is first induced with the negative voltage, orienting the dipoles to induce attractive force to the electrons forcing them to be fully depleted as shown in **Fig. 3(c)**. The reverse sweep is vice versa, inducing repulsive force from the ferroelectric dipoles making the electrons accumulate at the interface as shown in **Fig. 3 (d)**. (16,17) The device operates without forming a direct leakage current path through the ferroelectric layer. This can also improve the stability of the

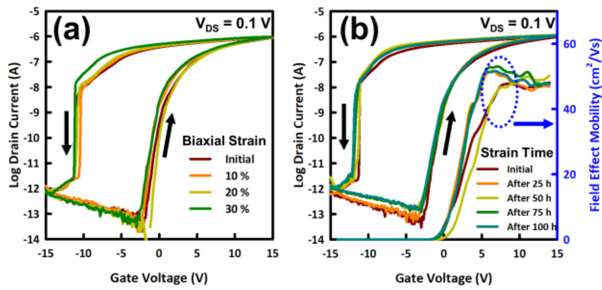

Figure 5. The stretchability of the FE-TFT on PI/PDMS substrate. Hysteresis curves of (b) the stretched FE-TFT up to 10% to 30% and (c) up to 100 h with the fixed biaxial strain of 30 %.

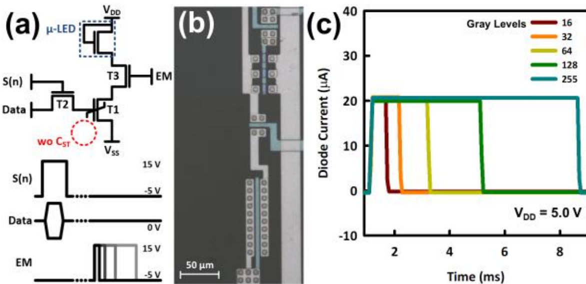

Figure 6. Display pixel application of the FE-TFT. (a) Pixel circuit and timing diagram of the 3T0C pixel with the FE-TFT working as a constant current part. (b) Optical image of the 3T0C circuit with the W/L = 30/6 μm of driving FE-TFT and W/L = 20/6 μm of SW-TFT. (c) The current measurement of the 3T0C pixel circuit

device. (16,17)

Bending and stretching tests were conducted on the FE-TFT to evaluate the mechanical stability. **Fig. 4(a)** shows hysteresis curves of the flexible FE-TFT of R = 5 mm, 3 mm, 2 mm, and 1 mm. **Fig. 4(b)** depicts hysteresis curves with 10000 cycles (R = 3 mm) of bending endurance. The device showed stable operation in both bending tests. The endurance and retention characteristics at R = 1 mm are shown in **Fig. 4(c) and (d)**, respectively. The endurance shows stable operation of up to 1000 cycles at a ± 15 V V_{GS} sweep. The retention characteristics show a slight increase in current, due to the depletion nature of the device. (17) **Table 1** summarizes the reported fluorite-based flexible FE-TFTs. The proposed device shows the lowest operatable bending radius. The FE-TFTs on the PI substrate were transferred onto the PDMS substrate to achieve stretchability. The detailed PDMS transfer process flow is demonstrated in our previous work. (13) The stretchability of the device was evaluated with the biaxial stretching test up to 30 % (**Fig. 5(a)**) and by maintaining 30 % biaxial strain for 100 h (**Fig. 5(b)**). The $\Delta\mu_{FE}$ showed a maximum of 7.9 % compared to the initial state, indicating the mechanical robustness of the FE-TFTs.

Fig. 6 shows the possible display application of the FE-TFT. **Fig. 6(a)** shows a circuit diagram of the proposed pixel circuit. The driving FE-TFT (T1) was utilized as the constant current generation (CCG) using the memory characteristics. SW-TFTs (T2, T3) were fabricated by removing the ferroelectric layer before active deposition. **Fig. 6(b)** shows the optical image of the fabricated 3T0C pixel circuit. The pulse width modulation (PWM) operation is displayed in **Fig. 6(c)**. The pulse width was modulated with a single EM transistor at this level. The current showed 20 μA of on-current at V_{DD} = 5.0 V, and the current was maintained throughout the measurements. Note that the current was maintained constantly without a storage capacitor. Although challenges remain in achieving individual pixel operation, the results demonstrate the possibility of FE-TFT replacing CCG components in PWM pixel circuits.

4. Conclusion

We proposed an MISF-structured FE-TFT on flexible & stretchable substrates. The FE-TFT showed 9.1 V of MW with ± 15 V V_{GS} sweep. The device operates by ferroelectric coupling without having the leakage current path through the FE layer. Mechanical tests confirmed robustness, with stable operation at R = 1 mm. The device maintained $\Delta\mu_{FE}$ < 7.9% under 30% biaxial strain for 100 h, validating its stretchability. Further, the 3T0C pixel circuit is proposed using the MISF device. The SW-TFTs were realized by etching the FE layer during the MISF process. The current remained stable throughout the measurements, suggesting the potential for replacing the CCG component in PWM pixel circuits.

5. Acknowledgements

This work was supported by the National Research Foundation of Korea (NRF) grant funded by the Korean government (MSIT) (No. 2020M3H4A1A02084899).

6. References

1. Hsain HA, Sharma P, Yu H, Jones JL, So F, Seidel, J. Enhanced piezoelectricity of thin film hafnia zirconia (HZO) by inorganic flexible substrates. Appl Phys Lett. 2018;113(2):022905
2. Liu WY, Liao JJ, Jiang J, Zhou YC, Chen Q, Mo ST, Yang Q, Peng QX, Jiang LM. Highly stable performance of flexible Hf0.6Zr0.4O2 ferroelectric thin films under multi-service conditions. J Mater Chem C. 2020;8: 3878--3886
3. Chen Y, Yang Y, Yuan P, Jiang P, Wang Y, Xu Y, Lv S, Ding Y, Dang Z, Gao Z, Gong T, Wang Y, Luo Q. Flexible $Hf_{0.5}Zr_{0.5}O_2$ ferroelectric thin films on polyimide with improved ferroelectricity and high flexibility. Nano Res. 2022;15:2913-2918
4. Liu B, Zhang Y, Zhang L, Yuan Q, Zhang W, Li Y. Excellent HZO ferroelectric thin films on flexible PET substrate. J Alloys Compd. 2022;919:165872
5. Liu H, Lu T, Li Y, Ju Z, Zhao R, Li J, Shao M, Zhang H, Liang R, Wang XR, Guo R, Chen J, Yang Y, Ren TL. Flexible Quasi-van der Waals Ferroelectric Hafnium-Based Oxide for Integrated High-Performance Nonvolatile Memory. Adv Sci. 2020;7(19):2001266
6. Islam MM, Hasan MM, Jang J. High-Performance Flexible Hf0.5Zr0.5O2 Ferroelectric Thin-Film Transistors on PI Substrate By Solution Process. ECS Meet Abstr. 2022;15:812
7. Li Q, Wang S, Li Z, Hu X, Liu Y, Yu J, Yang Y, Wang T, Meng J, Sun Q, Zhang DW, Chen L. High-performance ferroelectric field-effect transistors with ultra-thin indium tin oxide channels for flexible and transparent electronics. Nat Comm. 2024;15:2686
8. Kim DJ, Billah MM, Lee S, Siddk AB, Cho YJ, Jang J, Lee J, Lee Y, Shin J. Excellent Mechanical Durability of In-Folding Stress of Poly-Si Thin-Film Transistor on Plastic Substrate Compared with Out-Folding: Generation of Gate Leakage Currents in Flexible Poly-Si Thin-Film Transistor by Out-Folding and Bias-Temperature Stress. Adv Eng Mater. 2021;23(3):2000901

9. Mohit, Migita S, Ota H, Morita Y, Tokumitsu E. Thermal stability of ferroelectricity in hafnium–zirconium dioxide films deposited by sputtering and chemical solution deposition for oxide-channel ferroelectric-gate transistor applications. App Phys Express. 2021;14:041006.
10. Jung HS, Lee SA, Rha SH, Lee SY, Kim HK, Kim DH, Oh KH, Park JM, Kim WH, Song MW, Lee NI, Hwang CS. Impacts of Zr Composition in Hf1−xZrxOy Gate Dielectrics on Their Crystallization Behavior and Bias-Temperature-Instability Characteristics. IEEE Trans Electron Devices. 2011;58(7):2094- 2103.
11. Hasan MM, Roy S, Mohit, Tokumitsu E, Chu HY, Kim SC, Jang J. High performance, amorphous InGaZnO thin-film transistors with ferroelectric ZrO2 gate insulator by one step annealing. Appl Surf Sci. 2023;611:155533.
12. Starschich S, Schenk T, Schroeder U, Boettger U. Ferroelectric and piezoelectric properties of Hf1-xZrxO2 and pure ZrO2 films. Appl Phys Lett. 2017;18(110):182905.
13. Park C, Kim J, Lee H, Lee J, Islam MM, Jeong H, Jang J. Biaxially Stretchable Active-Matrix Micro-LED Display with Liquid Metal Interconnects. Adv Mater Technol. 2024;9(14):2301413
14. Joh H, Nam S, Jung M, Shin H, Cho S, Jeon S. Ferroelectric Hafnia-Based M3D FeTFTs Annealed at Extremely Low Temperatures and TCAM Cells for Computing-in-Memory Applications. IEEE Electron Device Lett. 2023;44(15):51339-51349
15. Hasan MM, Mohit, Islam MM, Bukke RM, Tokimitsu E, Chu HY, Kim SC, Jang J. Improvement of Amorphous InGaZnO Thin-Film Transistor With Ferroelectric ZrOx/HfZrO Gate Insulator by 2 Step Sequential Ar/O2 Treatment. IEEE Electron Device Lett. 2022;5(43):725-758
16. Mulaosmanovic H, Kleimaier D, Dunkel S, Beyer S, Mikolajick T, Slesazeck S. Ferroelectric transistors with asymmetric double gate for memory window exceeding 12 V and disturb-free read. Nanoscale. 2021;38(13):16258-16266
17. Lee H, Islam MM, Bae J, Jeong M, Roy S, Lim T, Rabbi MH, Jang J. A Coplanar Crystalline InGaO Thin Film Transistor with SiO2 Gate Insulator on ZrO2 Ferroelectric Layer: A New Ferroelectric TFT Structure. Adv Mater Technol. 2024;2401075